CHAPTER

2 Radio propagation modeling methods and tools

Katsuyuki Haneda[a,b], Richard Rudd[c], Enrico Vitucci[d], Danping He[e], Pekka Kyösti[f], Fredrik Tufvesson[g], Sana Salous[h], Yang Miao[i], Wout Joseph[j], and Emmeric Tanghe[j]

[a]*Aalto University, Espoo, Finland*
[c]*Plum Consulting, London, United Kingdom*
[d]*University of Bologna, Bologna, Italy*
[e]*Beijing Jiaotong University, Beijing, China*
[f]*University of Oulu, Oulu, Finland*
[g]*Lund University, Lund, Sweden*
[h]*University of Durham, Durham, United Kingdom*
[i]*University of Twente, Enschede, Netherlands*
[j]*Ghent University, Ghent, Belgium*

This chapter provides overview of fundamental definitions, tools, and new methods towards improved channel modeling reported in the Co-operation in Science and Technology (COST)-Inclusive Radio Communications (IRACON) Action for future wireless communications and networks. The overview first covers definitions of *propagation environments* as they determine most relevant propagation mechanisms to consider and model, and furthermore, guide our approach to channel modeling methods. This chapter then introduces new insights into popular approaches of channel modeling, i.e., *site-specific and geometry-based stochastic channel modeling*, where the latter particularly features canonical and standardized channel modeling approaches taken by the 3rd Generation Partnership Project (3GPP), COST, and International Telecommunication Union (ITU) communities. Finally, this chapter shed lights on new modeling approaches to *small-scale radio propagation behaviors*, covering plane wave propagation paths and distributed diffuse scattering.

[b] Chapter editor.

Inclusive Radio Communications for 5G and Beyond. https://doi.org/10.1016/B978-0-12-820581-5.00008-0

2.1 Propagation environments

2.1.1 Introduction

Let us first put propagation environments in the context of the history of wireless communications so that the contributions of the COST-IRACON action become clear. The first experimental work on radio channels, by the likes of Hertz [CW95] and Bose [Eme97] was carried out over very short paths using ultra high frequency or microwave radiation in an indoor environment. The utility of lower frequencies was soon discovered by workers such as Marconi and for many years the focus shifted to much lower frequencies and paths of tens or hundreds of kilometers. The available bandwidth was very small and multipath effects only became noticeable in the context of ionospheric propagation. With the advent of television, wideband telephony, and data in the mid-twentieth century, higher frequencies were re-visited and it became necessary to pay attention to the dispersive nature of the radio channel. With the quest for bandwidth, carrier frequencies continued to rise and the millimeter wavelengths pioneered by Bose are now the subject of intense study in the context of 5G communications. The aim of the radio propagation activities within the COST-IRACON action has been to support the goal of 'inclusive' use of wireless connectivity in all environments by the development of improved channel models. Whereas traditional radio systems were required to address a fairly limited range of topologies (e.g., broadcast transmission from high sites to rooftop antennas, cellular base stations to hand-held terminals, a wireless LAN router to nomadic terminals within a building), future systems will be expected to accommodate a much more heterogeneous range of channels; this variety is reflected in the propagation environments that have been subject to scrutiny within the COST-IRACON action.

2.1.2 Outdoor environment

Historically, it has been the outdoor channel that has received most attention, with most early modeling effort concentrating on characterizing path loss using empirical expressions such as those due to Okumura [OOKF68] and Hata [Hat80]. Semi-deterministic models [Bul47,Dey66] attempted to account for diffraction around major terrain features, but local signal variability due to shadowing by trees, buildings, and other 'clutter' could only be treated statistically, with this 'location variability' generally characterized as a log-normal distribution. The 'physical-statistical' approach blends predicable physical effects, such as rooftop diffraction or reflection from walls, with statistical data such as building heights and orientation, to give simple but efficient models [WB88] as illustrated in Fig. 2.1.

With the advent of digital mobile communication, the wideband characteristics of the channel started to attract attention [Cox72]. Characterizing multipath with ever-greater resolution has been a focus for the last decades, first in two dimensions and now in three, as smaller operating wavelengths and greater computing power have enabled highly directional, dynamically-synthesized antenna beams to be realized. Much of the current work still centers on the statistical characterization, by measure-

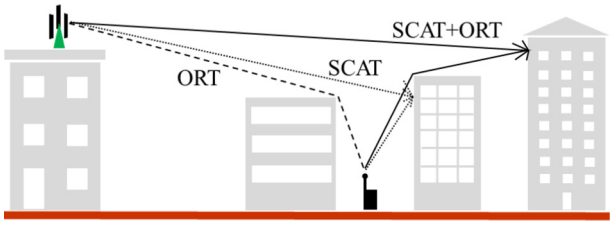

FIGURE 2.1

Contribution of scattered (SCAT) and over-roof-top (ORT) signals [VFB+18].

ment, of the spatial channel; such studies are, however, time-consuming and, with the recent explosion in the availability of high-resolution environmental data, the use of deterministic models to explore and characterize the channel is attractive. At lower frequencies, it is reasonable to expect that bulk diffraction effects due to buildings can be modeled with some accuracy as vector representations of the built environment are widely available.

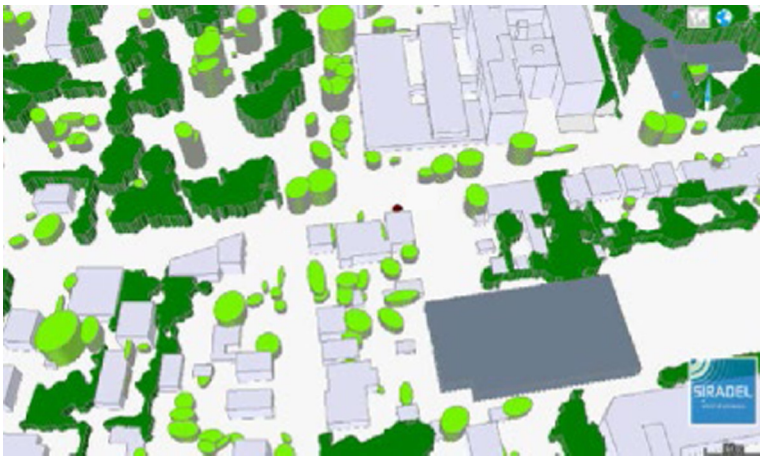

FIGURE 2.2

Vector representation of buildings and vegetation [CTS+16].

Major challenges remain, however, in characterizing building materials in terms of their electrical constants and surface roughness [FPK+18], both important for the modeling of reflection and scattering and hence of the multipath environment. Similarly, vegetation is inevitably less well described in environmental databases (although the situation is improving) and will often need to be treated statistically as exemplified in Fig. 2.2.

2.1.3 Indoor environment

The highest-bandwidth wireless services are disproportionately consumed in indoor environments. The indoor propagation channel is generally very dispersive with metal structures and fittings giving rise to a rich variety of clustered multipath components that can be problematic for increasingly broadband channels; a visual representation of multipath power arrival profile is shown in Fig. 2.3 [KIU+20]. While the outdoor environment is clearly varied, indoor spaces are even more diverse as seen in channels of a small domestic room, a factory, a tunnel, and an airport expected to show very different behavior. The sheer variety of indoor environments makes characterization by simple statistical models challenging. Deterministic approaches, such as ray tracing or even full-field methods [MVB+18] are attractive because of the limited dimensions, and hence modest computational effort involved. Set against this, however, is the same problem as mentioned in Section 2.1.2 of obtaining sufficiently detailed data on the constituent materials and their electrical properties. Moreover, items such as furniture may move (and are unlikely to be included in computer-aided design models), while human bodies may significantly change the RF environment. For the most part, it is unlikely that prediction models will be used for the operational planning of indoor radio networks; much work is therefore aimed at the development of statistical models for use in physical layer design and standardization activities. With the trend towards increasing system bandwidths, understanding the distribution and clustering of multipath components is a major area of research, while the drive to exploit higher frequencies has led to debate, and conflicting evidence, regarding the frequency dependence of Diffuse Scattering (DiS).

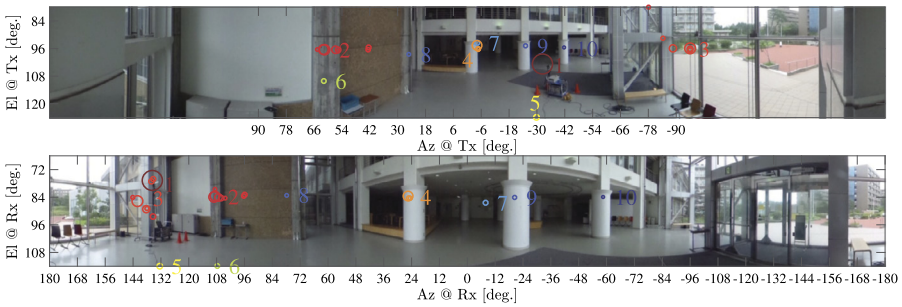

FIGURE 2.3

Visualization of spatial energy distribution in an indoor environment [KIU+20].

2.1.4 Outdoor-to-indoor environment

There is an increasing expectation that radio systems will provide seamless connectivity as the user moves in and out of buildings. The ability to make realistic

predictions of the loss suffered by signals penetrating building fabric is therefore important not only for the estimation of the indoor service that may be provided by outdoor base stations, but also in the assessment of interference between systems located on different sides of the indoor-outdoor interface. It is therefore unfortunate that building loss is poorly-characterized, partly due to the wide variability within and between buildings. Concern has also been expressed that the increased use of energy-efficient construction practices may be causing building entry loss to increase [Han16].

Previous work [RML+18] has shown that the trend of loss with frequency is non-monotonic, with the lowest and highest frequencies suffering the greatest loss, presumably due to the small size of building apertures in terms of wavelength at the low-frequency end, and the generally higher material absorption rate at the higher end. While the behavior of specific building materials (brick, concrete, glass, etc) has been well characterized in isolation, using this data to predict large-scale building entry loss is not trivial. Even very small gaps in structures can have a large and frequency-dependent impact, and windows with multiple glazing can form band-stop filters as exemplified in Fig. 2.4 [KLHNK+18].

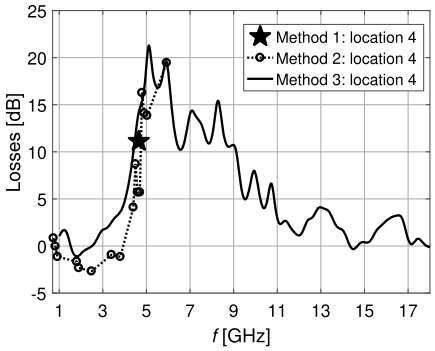

FIGURE 2.4

Double-glazed window as bandstop filter [KLHNK+18].

2.1.5 Train and other vehicular environments

Vehicle connectivity has become an important application area for 5G systems; beyond the obvious opportunities for delivering high bandwidth content to rail passengers, the promised ubiquity and low-latency of such systems will be a key enabling technology for assisted-driving or self-driving cars. This has inspired much recent work to characterize the Vehicle-to-Infrastructure (V2I) and Vehicle-to-Vehicle (V2V) channels, as detailed in Section 3.4. Such channels are very dynamic and characterized by large, and rapidly-changing Doppler shift. The condensed parameters of the railway channel change very rapidly between environments, e.g., from railway cuttings to viaducts, to tunnels and stations, as exemplified in Figs. 2.5 and 2.6.

Much attention has therefore been paid to the modeling of these dynamics within the COST-IRACON action.

FIGURE 2.5

Showing the diversity of railway environments [AHZ+12].

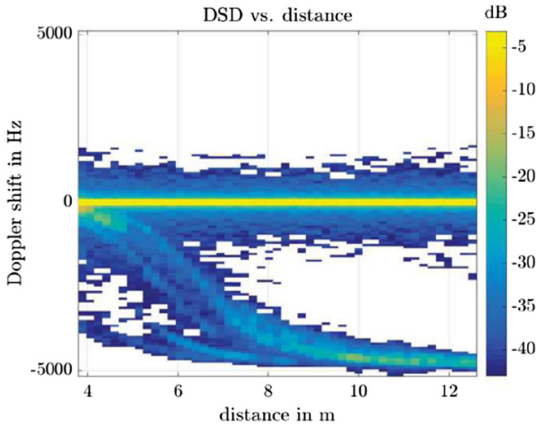

FIGURE 2.6

Rapid change to Doppler spectrum for railway channel [ZHL+18].

2.1.6 Body-centric environments

The on-body channel is very different from most other cases. Interaction between the antenna and the propagation environment is more apparent and may not be separable. On-body propagation at low frequencies is mainly due to creeping diffracted waves and penetration through biological tissue, both of which can be hard to characterize, leading to most works relying on empirical evidence. Body-to-body and body-to-infrastructure channels are similar to those in indoor scenarios, with added variability due to the body motion and installed antenna performance, e.g., [TCB19].

2.2 Channel model classification

Among diverse channel models and approaches, this subsection reviews the most popular ones in the scientific community as well as those for industrial standardization. The channel modeling methods and approaches decide their applicability and hence purposes, as detailed in each category of channel model hereinafter. The first approach to review is site-specific channel models which are mainly intended for coverage estimates when wireless network is deployed at a particular site. Stochastic models are then following where the main goal is comparison of physical layer proposals and inter-system interference analysis. The stochastic models do not aim at reproducing channel responses at a particular site but something plausible and realistic given an imaginary environment. They are therefore often called reference models. Different examples of reference models are introduced, including the ITU-R pathloss models, 3GPP and COST models.

2.2.1 Site-specific channel models

IRACON activities regarding site-specific model are presented here. In this context, the majority of the studies have been conducted in the field of ray models, which represent a good compromise between accuracy and computation time. Deterministic RF propagation prediction models using ray-optical approximations have been studied and tested with success since the nineties. More recently, due to the advent of MIMO transmission schemes and to the use of higher frequency bands in 5G-and-beyond communication systems, ray models have gained popularity and have been proposed for a variety of uses, including the design and planning of mobile radio systems and services, fingerprinting and multipath-based localization methods, or real-time use for the optimization of wireless systems performance. In serving all these purposes, there are technical challenges in ray-based models as outlined in the following.

- *Computation time:* despite the various approximations of radio wave propagation behavior that are considered, and the always-increasing computation efficiency of modern computers, the required scale of the radio channel simulations can easily go beyond the capability of the presently available computational resources.
- *Description of the environment:* the approach of ray-based models is necessarily deterministic or quasi-deterministic, therefore an accurate knowledge of the environment is needed, usually in terms of 3D digital maps. But there are often practical problems in having all the environment information stated deterministically, leading thus either to simplifications in the modeling, or to the use of stochastic modeling methods. On the other hand, point-cloud maps obtained through laser scanning are nowadays widely available for different kind of environments, and their use can be leveraged to develop new models with a reasonable compromise between complexity and accuracy.
- *Application to complex environments and higher frequency bands:* new channel models need to support 5G-and-beyond technologies such as Massive MIMO and

hybrid beamforming, among others, in a wide variety of settings, including the use of millimeter-wave frequencies and also in new applications and link types, such as Device-to-Device (D2D), vehicle-to-everything (V2X), and air-to-everything (A2X).

The following subsections introduce activities in COST-IRACON to address the mentioned technical challenges, with particular reference to ray models. Latest developments regarding the use of deterministic and physics-based models other than ray-based models, such as full-wave models, are also outlined at the end of the section.

2.2.1.1 Acceleration techniques for ray-based models

In order to cope with the high computation time of for Ray Tracing (RT) and ray launching models, novel efficient algorithms and acceleration techniques have been introduced.

2.2.1.1.1 Reduction of image trees

An efficient image-based RT algorithm is presented in [HB16]. The efficient implementation is thanks to reduction of the size of an image tree for tracing rays to a given mobile location, in addition to a fast ray-object intersection test method. The visibility region of an image can be represented by so-called lit polygons, and the buildings within this lit region will block the rays to form shadow regions as well as the higher order images, as shown in Fig. 2.7. Lit polygons can also be exploited to accelerate finding rays when a mobile is on a linear route. If entry and exit points of a mobile into the lit region can be identified, they make it unnecessary to perform geometrical check of meaningful polygons during the mobile is in the lit region.

2.2.1.1.2 Acceleration based on graph representation

Propagation environments and their interaction with radio waves are represented as a graph in RT according to [ALU16]. The use of the graph accelerates and simplifies the ray tracing process.

2.2.1.1.3 Acceleration based on preprocessing

Analyzing visibility between all surfaces inside a scenario allows acceleration of ray-optical multipath propagation simulations for path loss predictions, according to [DK19]. The visibility preprocessing is formulated through a Surface Relation Tree (SRT), which stores the relation between all surfaces in the scenario, and a Location Surface Tree (LST), which is used by the Raytracer to determine visible surfaces for any given location in the scenario, as outline in Fig. 2.8. The visibility relations between surfaces are represented as polygons similarly to Fig. 2.7. This allows to transform most needed calculations of LOS-check into a point-in-polygon-problem that can be solved by an efficient algorithm. This approach also applies to scenarios with moving devices.

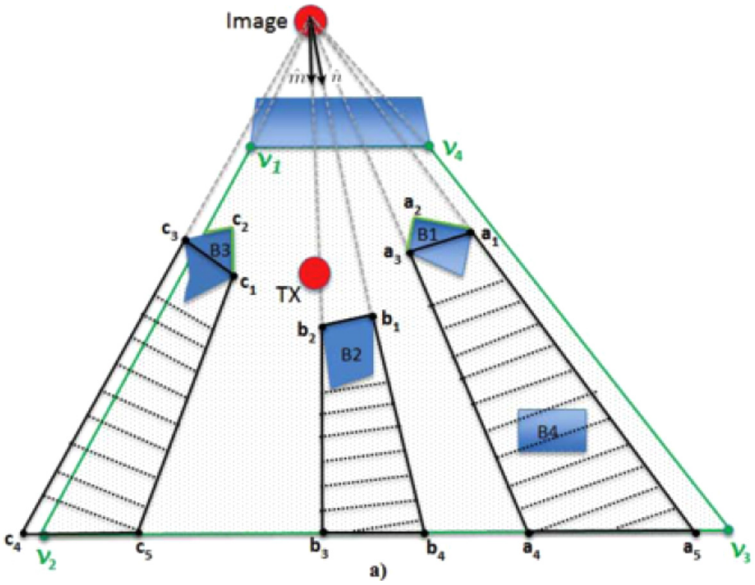

FIGURE 2.7

Lit and shadow polygon of a reflection image [HB16].

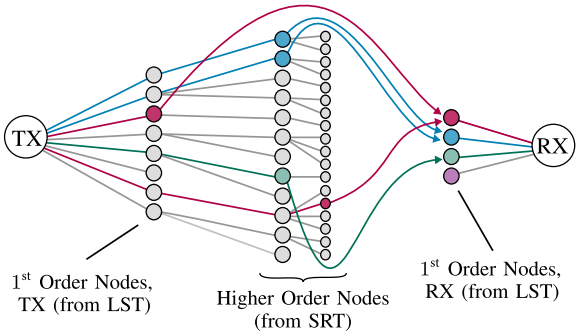

FIGURE 2.8

A set of surfaces represented by the first-order nodes looked up in the LST is visible by each Tx and Rx. The SRT is then used to find other visible surfaces leading to higher order nodes and to set up a visibility graph. It is finally used to determine a connection from the Tx-node to the Rx-node [DK19].

2.2.1.1.4 Discrete ray launching with visibility preprocessing and GPU parallelization

The preprocessing of environment visibility is also shown to facilitate faster geometric computations for both specular and diffuse interactions, according to Lu and Degli-Esposti [LVD+19,DLV+18]. They call it a fully Discrete, Environment-

Driven, Ray Launching (DED-RL) field prediction algorithm. The environment is discretized into simple regular shapes (tiles), which allows for visibility preprocessing and straightforward parallelization of the algorithm on NVIDIA-compatible Graphics Processing Units (GPUs). All the visibility relations among tiles ares stored in a visibility matrix, then ray tubes are launched toward each tile visible from the Tx and then bounced towards the other tiles with the aid of the pre-computed visibility matrix. Both the visibility matrix creation and bouncing procedure are parallelized. Combining these innovative features boosts the computation speed of up to 4 orders of magnitude compared to a standard image-RT algorithm as evidenced in Fig. 2.9. Despite the significant speed-up, DED-RL retains the same level of prediction accuracy as image-RT tool with respect to RF coverage measurements.

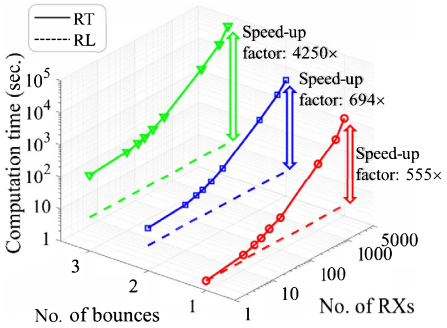

FIGURE 2.9

Computation times and speed up factors of DED-RL with respect to non-parallelized Image-RT in a dense urban scenario (Union Square, San Francisco, USA), for different number of bounces. Computation times of DED-RL are represented with dashed lines [LVD+19,DLV+18].

2.2.1.1.5 Parallelization with the aid of cloud HPC platforms

Parallelization of ray-path identification has obvious improvements in computational run-time. He et al. [HAG+19] implemented a parallel computing technology where High Performance Computing (HPC) in the cloud is used with several computing nodes involving Central Processing Unit (CPU) and Graphics Processing Unit (GPU). Their high-performance cloud-based RT simulation platform (CloudRT) has an architecture illustrated in Fig. 2.10, which is publicly available at http://www.raytracer.cloud/.

2.2.1.2 Applications of ray-optical wave propagation simulation methods to important systems and use cases of 5G cellular

Ray-based wave propagation models are applied to studies of a number of systems and use cases of 5G cellular. The systems include mm-wave and massive MIMO, while use cases usually refer to complex ones of outdoor, indoor, outdoor-to-indoor, vehicular, and air-to-ground scenarios. Ray-based wave propagation simulations

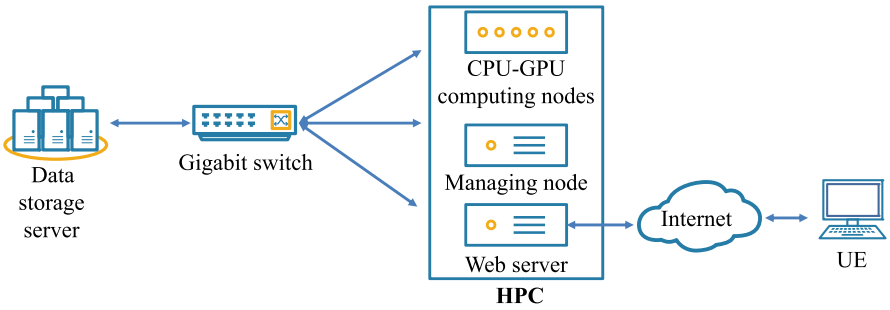

FIGURE 2.10

Network architecture of CloudRT [HAG+19].

sometimes complement measurements where channel sounding is not straightforward due to complexity of the cellular scenarios.

2.2.1.2.1 Application to mmWave frequencies

One of the distinguishing features of 5G cellular is the use of mmWave frequencies. Given the scarcity of understanding and measurements of cellular multipath channels at these frequencies, various efforts have been made in COST-IRACON action to gain more understanding about them through implementing ray-optical wave propagation models. For example, Corre et al. highlighted differences of wave propagation characteristics between mmWave and sub-6 GHz bands [CTS+16] and furthermore studied multipath propagation characteristics at frequencies above 90 GHz [DCB+18]. The former study mentions the importance of considering vegetation into the simulations, while the latter covering indoor and outdoor radio propagation shows that not only the frequency and antenna type, but also the properties of objects such as wall and furniture have significant impact on the channel features. Aslam et al. report a ray-based model implementation for the assessment of a 60 GHz outdoor small-cell networks [CACL17]. Multipaths are predicted from interactions with the static environment, but also with randomly-positioned vehicles and user-bodies causing ray-path blockage and new propagation paths. Importance of considering small physical objects that may cause shadowing and scattering, e.g., parked cars and lamp-posts, was also pointed out in [MVB+18] according to their outdoor RT model run at 26 GHz and 38 GHz. The results show that, in non-line-of-sight conditions, the contribution from non-specular components, even at these frequencies, is determinant to have a good prediction accuracy of measured pathloss.

2.2.1.2.2 Application to a wave propagation study in complex environments

Ray-based wave propagation models also help studying multipath channel characteristics where measurements may not always be feasible. Degli-Esposti et al. study for example power-Doppler-profiles of a highly dynamic vehicular radio communication

link. Their dynamic ray tracing model provides multidimensional channel prediction in any instant within a channel's coherence time. Other typical dynamic scenario of interest is air-to-ground (A2G) radio communications for Unmanned Aerial Vehicles (UAV). Vitucci et al. investigate the A2G channel in a reference urban scenario by means of the powerful DED-RL tool introduced earlier in this section [AVB+19]. Due to its computational efficiency, it is possible for the tool to cover a quite wide urban area, providing a large data-set for statistical assessment of A2G propagation and the optimization of drone trajectories.

Large-scale simulations of wave propagation, e.g., across a city for cellular coverage study, are another typical example where measurement-based analysis may practically be infeasible. A research group of Degli-Esposti and Vitucci made pioneering efforts in large-scale wave propagation simulations. For example, a hybrid method of deterministic 3D outdoor multipath prediction and its indoor extension using a radiosity-based method allows efficient computation of indoor coverage as demonstrated in [LVD+19]. The ray-tracer calculates received field strength on building surfaces, while the radiosity method extends the analysis to indoor using volume information of buildings. The hybrid method works well for indoor coverage estimation in high-rise buildings, where a 3D outdoor map of buildings is readily available but the detailed indoor map of the building is unknown. In a separate work [VFB+18], Over-Roof-Top (ORT) propagation in dense urban environment is investigated. ORT propagation is known to provide energy to mobiles when a base station is elevated above rooftop to cover a wide area of a built environment. Standard ORT models of wave propagation based on multiple diffracting knife-edge modeling of a series of building are considered, in addition to possible reduction of diffracting edges and consideration of heuristic correction factors. Results show that standard ORT models generally overestimate the attenuation, while their combination with edge reduction and correction factors improve coverage prediction accuracy.

2.2.1.2.3 Elaborated diffuse scattering models

In recent years, several works have shown the importance of DiS to achieve accurate prediction of the radio channel characteristics in real propagation environments. The importance is verified through a series of analyses of measured multipath channels where specular wave propagation such as reflection and diffraction does not account for all the power delivered to the receiver from the transmitter. DiS models are often embedded into ray tracing in order to consider the effect of surface roughness and other irregularities which cannot be modeled in a fully deterministic way. The models can either be built by highlighting their micro- or macroscopic nature. Microscopic models to represent DiS include Lambertian, directive, and backscattering models [EFVG07]. As depicted in Fig. 2.11, the scattered field is directed to the normal direction of a surface in the Lambertian model, while it is directed to the direction of specular reflection in the directive model. Examples of DiS models from macroscopic perspectives are elaborated in Section 2.2.5.

Improved mathematical models of microscopic DiS were proposed in the COST-IRACON action. For example, Wagen [Wag19b] introduces a formulation of scat-

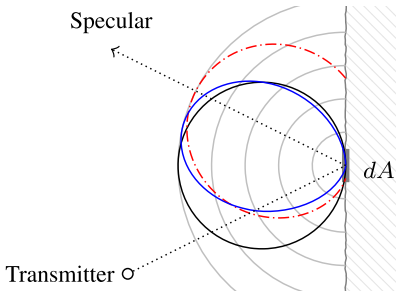

FIGURE 2.11

Polar plot of scattered power at one tile for an impinging path at 30°: the Lambertian model is in black, the Directive model is in red (mid gray dash-dotted line in print version), and the dotted arrow denotes a specular reflection pathway [KWG+18].

tered fields accounting for both specular reflection and DiS. It satisfies the Helmholtz reciprocity principle, has dependency on distances between a scatterer and field transmit/receive points and finally takes into account the facet size from smooth to rough surfaces. Freire et al. [FPK+18] test if the Kirchhoff theory can provide reasonable estimation of scattered fields from a rough surface when surface shadowing may not be negligible. Such shadowing matters when a surface roughness is greater than a wavelength of radio signals. According to measured DiS from a rough brick wall at 60 GHz, surface shadowing effects were found to have moderate influence and the Kirchhoff theory brought good prediction accuracy of scattered fields from the rough wall.

2.2.1.2.4 Application to massive MIMO channel modeling

Another important aspect of future communication systems is the use of very large antenna arrays to take advantage of beamforming technology in multi-user scenarios, commonly known as massive MIMO. Ray models are particularly suitable to evaluate the performance of MIMO systems for various channel conditions and antenna configurations. However, one peculiarity to apply the ray models to a very large array is the validity of a plane wave incident model of a ray when a scatterer is close to the array. Zentner et al. [ZMM17] therefore studied the validity of the plane wave model for polarization, radio frequency and the sizes of antenna arrays at both sides of communication channel. Another peculiarity of massive MIMO channels is the fact that different parts of a single large antenna array may see different scattering environment and hence rays. This peculiarity was addressed by Sayer et al. [SBHN19]. They found that properties of ray-paths traced from a single transmit antenna element to a single receive antenna element, both in a large antenna array, can be different from those traced between the center of each antenna array. More accurate MIMO channel matrices can be obtained by the RT between individual antenna elements in arrays at link ends, though computational load increases. A possible compromise to keep both accuracy and computational load reasonable may be to trace rays for a vertical col-

umn of antenna elements only once using its center coordinate, while rays are traced for each element across horizontal row of antennas. Considering these peculiarities allows for realistic evaluation of radio network performance using RT. For example, Aslam et al. [ACBL18a] reported the system-level performance of a 16-macro-cell MIMO network in outdoor environment. Array configurations at the massive base station array showed significant impacts on the system-level performance.

2.2.1.3 Use of maps and point-clouds for ray-optical propagation modeling

Digital maps of the environment are the natural input for most site-specific propagation modeling, like ray tracing. However, there are also challenges of using digital maps for demanding air interface evaluations because there are currently no open source digital 3D map material that includes all features required for successful radio propagation simulations [HHS18]. The same work showed that a database containing all the needed information can be built from multiple sources for simulation use. In the following work, a novel method to join maps with different coordinate systems together is introduced [SHP+18]. The combined map is useful for site-specific propagation modeling and their visualization on a three-dimensional environment.

Describing the environment using point clouds, an example shown in Fig. 2.12, is another promising method for wave propagation simulations. They are obtained through laser scanning or photogrammetric survey of the physical environment. Proper modeling of propagation mechanisms for point clouds allows accurate simulation of multipath channels, as summarized in the following.

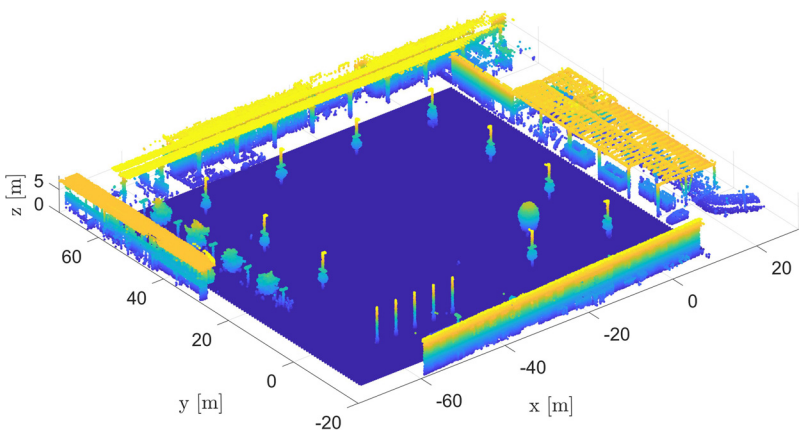

FIGURE 2.12

A sample point cloud of an open square [KSH19]. Points are colored according to their heights above the floor.

2.2.1.3.1 Wave-object interaction analysis based on point clouds

Wagen et al. [WVH16,Wag17,Wag18,WK18a,WK18b,Wag19a] made several contributions to radio propagation simulations using point clouds:

- *Simulation of specular reflection, scattering, and diffraction:* [WVH16] proposed a formulation of the specular reflection for point clouds. The model is verified with a reflection measurement from a small metal surface in an anechoic chamber at 15 GHz RF. The measurement shows that the specular reflected field was observed mainly from the illumination of about a third of the metal surface; [Wag17] illustrates simple mathematical models for simulating scattering and diffraction. Thereafter, [Wag19a] computes the scattering and specular reflection components using a single formulation, instead of accounting for them separately.
- *Application to large-area simulations:* [Wag17] uses detailed topographical data available in Switzerland in the form of point cloud for propagation simulations. Comparisons between the simulations and the wideband impulse response measurements at 69 and 254 MHz show that the dominant channel responses can be reproduced; [Wag18], [WK18a], and [WK18b] compare simulated and measured multipath channels using delay spread and a new metric called channel rise time.
- *Application to small-cell scenarios:* Comparisons of simulated and measured channels were reported in [WK18a] for 5 GHz WiFi connectivity in indoor and outdoor picocells. The work [WK18b] provides more comparisons in terms of spatial fading and data loss rate.
- The mentioned works highlight two potential challenges for propagation modeling using point clouds: (1) identifying long-delayed multipaths with up to a hundred of microseconds or more and (2) defining objective measures to rank the accuracy of different propagation models.

2.2.1.3.2 Use of point clouds for above-6 GHz radio channel modeling

As point cloud description of physical environments preserves small details such as lampposts and roughness in facade in outdoor environments and tables and chairs in indoor scenarios, it is particularly useful in site-specific propagation modeling at above-6 GHz RF where their wavelength is comparable to the details. A ray-tracer implementing all relevant propagation mechanisms including specular reflections, DiS, diffraction and shadowing is applied to an indoor point cloud, showing its validity at 60 GHz band in [JHK16]. In applying the point cloud data to above-6 GHz propagation channel modeling, a particular attention goes to pre-processing techniques of point clouds as they may not be applicable to RT as such. For example, Pascual-Garcia et al. [PGMGPMI+18] show a novel algorithm to extract a geometrical model from point clouds. Flat rectangular surfaces are extracted from a point cloud to produce a complete surface model of the environment, which is used in a ray tracing tool to conveniently estimate the specular and the diffuse components. The technique applied to an indoor environment demonstrates that the obtained surface model contains the needed detail to yield a good level of accuracy in wireless channel simulations. Koivumäki et al. [KSH19] compare multipath channels simulated

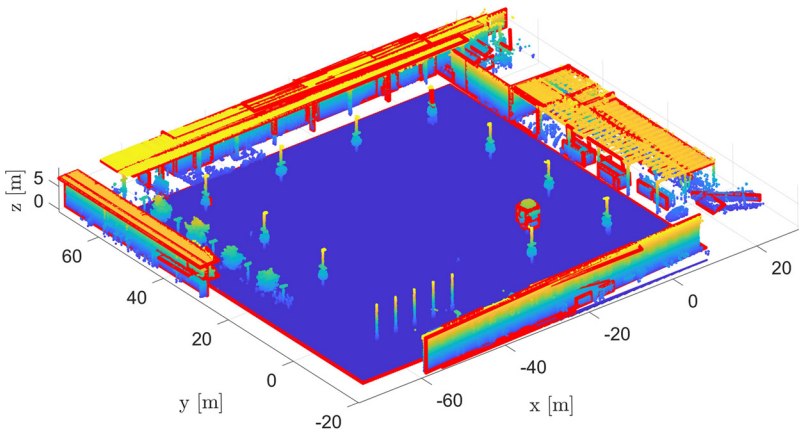

FIGURE 2.13

Processed point cloud after the de-noising, grouping, and filling that preserve details; original one is shown in Fig. 2.12. Wedges are detected for diffraction simulations as presented in red [KSH19].

from ray tracing using point clouds with different pre-processing techniques applied. Their results indicate that preserving small details of the environment is important for accurate ray-based radio propagation simulations. Proper processing of point clouds, which includes de-noising and wedges detection as shown in Fig. 2.13, led to the best accuracy in simulating physical propagation paths of the measured channels.

2.2.1.4 Full-wave models and other physics-based models

Steady increase of available computational power in CPU and GPU makes it feasible to solve electromagnetic fields of a radio environment using full-wave method. Despite being much more computationally demanding than ray-based method, it has a potential to provide very accurate results, and furthermore can also complement ray models. Analyses of scattering due to cluttering and vegetation are good examples where full-wave analysis can provide better understanding, and hence provide better mathematical models that can be incorporated into ray models.

2.2.1.4.1 Volume electric field integral equation

Kavanagh et al. solve the volume electric field integral equation (VEFIE) for indoor environments [KB19]. Comparison between two- and three-dimensional solutions of the equation reveals tradeoff between computational load and accuracy of the solutions. For a wideband channel simulation, it is necessary to solve the integral equation over a range of frequencies. Lin et al. [LAG+18] made an interesting comparison between solutions of the VEFIE and RT along with measured channels in an indoor environment. Estimated received power levels are shown in Fig. 2.14. The plot indicates that optimized RT achieved the highest accuracy in estimating received power level, while a good compromise between computation time and accuracy is found

by the 2D VEFIE with a heuristic path loss correction factor. The two-dimensional VEFIE solver was faster in field calculation than RT.

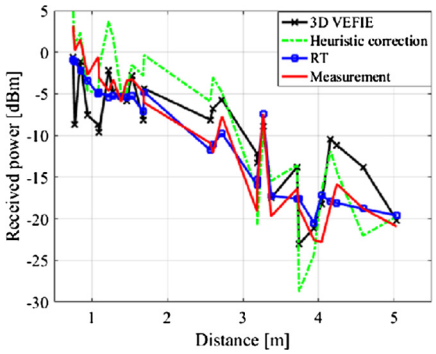

FIGURE 2.14

Received power estimated from 3D VEFIE, its heuristic correction and RT, compared against measurements [LAG+18].

2.2.1.4.2 Method of moments

Another popular full-wave method solver applied to electromagnetic scattering problems and wave propagation studies is the method of moments (MoM). For example, the method was applied to compute EM scattering from rough surfaces with Gaussian or exponential roughness profiles [PTCB15]; field distributions in indoor two-dimensional scenarios were solved using the method in [POC19] in order to study human blockage effects in beamformed 60 GHz radio channels.

2.2.1.4.3 Physical optics

The last method introduced in this subsection is physical optics (PO). PO [And96] is the high frequency approximation of the full-wave model in the lit region of a source, and has wide applicability for scatterers with different shapes and materials. It was originally developed for analyzing scattering from perfect electric conductor, but the concept of currents approximation is general and applicable to magnetic conductors, dielectric materials, and bodies with surface impedance [GMMLLH11]. PO takes less computation time compared to other rigorous numerical approaches where the induced currents on scatterer surface are determined by a large set of linear equations and could be extremely time-consuming to solve. The major source of errors in PO is at the edge of surface, or when the surface curvature is large and multiple reflection occurs. Gueuning et al. [GCO17,GCO19] used PO for fast computation of the near-field radiation from a planar object. The computation took advantage of an non-equispaced Fast Fourier Transform to convert from spatial to complex spectral domains.

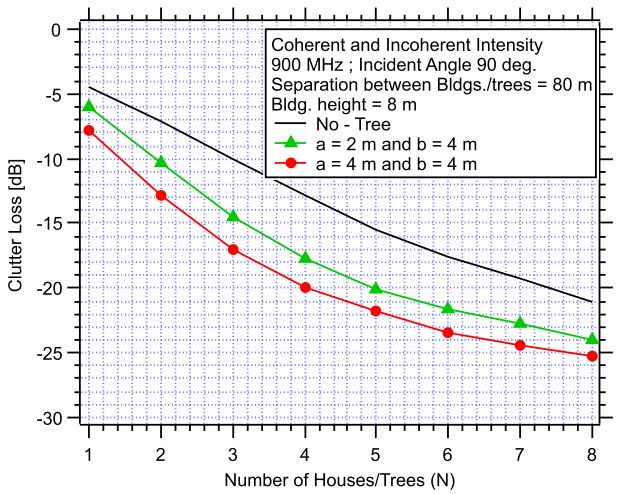

FIGURE 2.15

Clutter loss for vertically polarized fields at the top of the houses/trees for different tree widths a; b is a height of the elliptic model of leaves in a tree [TL18].

2.2.1.4.4 Physics-based model for path loss prediction in vegetated areas

Finally, for outdoor macrocellular wireless links, it is important to consider diffraction and penetration through vegetation and houses. Physics-based models to analyze path loss for such links have been studied for a long time, but still require further improvement. One of existing models is a Torrico-Bertoni-Lang model [TBL98]. It considers a row of houses or buildings, each of which is modeled by an absorbing screen. Each screen is topped with a canopy of trees modeled by a partially absorbing phase screen. Properties of the phase screens are determined to simulate the mean field in the canopy of the tree. PO is then used to evaluate the field at the receiver by using a multiple Kirchhoff-Huygens integration for each screen. The model is extended in [TL19] to reproduce measurements of the propagation loss for point-to-point systems at 3.5 GHz and 5.8 GHz in a vegetated residential area. The attenuation and phase delay of the mean field propagating through the tree canopy are evaluated using a random media model. Another extension is a physics-based model of clutter loss in a vegetated residential environment [TL18]. The improved model of the clutter loss adds the incoherent intensity of the received field produced by multiple trees/houses to the coherent intensity of the same. Estimated clutter losses in Fig. 2.15 show that fields scattered by the first few houses/trees seen from the base station led to both coherent and incoherent components and increased the losses. This observation is important for 5G mobile wireless systems since the size of the cells is few hundred meters; underestimating the clutter loss may result in an overestimation of cell size. Finally, the work [SUL19] is dedicated to accurate prediction propagation loss in a trunk dominated forest as an important application of Wireless Sensor Network

(WSN) to forested areas. A two-dimensional Radiative Transfer Equation (RTE) is solved for a plane wave incident on a trunk-dominated forest. The solutions of RTE are used to compute attenuation constants of both the coherent and the incoherent components. It is noted that at low frequencies, only the coherent intensity needs to be considered. As the frequency increases, the incoherent intensity becomes more important than the coherent intensity. Furthermore, as the transmit-receive distance increases, the coherent intensity decreases.

2.2.2 Geometry-based stochastic channel models (GSCM)

2.2.2.1 GSCM and their features

The family of Geometry-based Stochastic Channel Model (GSCM) has been widely used for physical layer standardization. It has a long history of development throughout the COST models, the 3GPP Spatial Channel Model (SCM), Wireless World Initiative New Radio (WINNER), IMT-Advanced (IMT-A) to recent 3GPP Three-Dimensional (3-D) and the latest 3GPP 5G channel models. The characteristics of GSCM can be defined from multiple features. Generally, the model is a GSCM if it has three characteristic features. Firstly, multipath propagation parameters contain *geometrical* definition of the environment, either in the angular domain or in the Cartesian coordinate system. Secondly, propagation parameters are at least partially *stochastic* and specified by probability distributions. Thirdly, the model enables consideration of realistic antenna characteristics by embedding of antenna radiation patterns sampled in the angular domain.

GSCMs in wireless standards have additional features. They all share close to identical mathematical frameworks and an algorithmic description for generating time-variant MIMO channel matrices containing transfer functions. The first feature is mostly limited to the angular domain, i.e., in the mentioned list of GSCMs the Multipath Component (MPC) or so-called clusters do not have locations but only directions (except for the COST2100 model where clusters are defined in the coordinate system). As a fourth feature, the path loss and shadowing are modeled by separate functions, where path loss model is an empirical function of at least the carrier frequency and the link distance, and the shadowing is a log-Normal zero-mean random process. Finally, these standard GSCMs contain the drop or the channel segment concept. Its essential feature is the so-called virtual motion, that provides Doppler shifts and temporal fading, but keeps all propagation parameters quasi-static and ensures Wide-Sense Stationary (WSS) for a small-scale movement of a mobile device.

2.2.2.2 Requirements for 5G channel models are still not fulfilled in the 3GPP model

Several channel modeling activities targeting 5G evaluations were completed, like European METIS [RKKe15] and mmMagic [Pet17] projects, before 3GPP started specifying its 5G channel model. In these projects, the first step was to envision functionalities of 5G networks and air interfaces, and to identify the new requirements set to channel modeling. These requirements are discussed in several articles, e.g.,

in [MKK+16]. The key drivers for 5G channel models are: large antenna arrays, new frequency bands, and new deployment scenarios of transceivers. A comprehensive gap analysis for upgrading 3GPP 3-D [36.15] to the 5G model (now [3GP17b]), based on the identified requirements, is performed in [JS16]. In total 17 categories of inaccuracies were found in the 3GPP 3-D model. Many problems were identified, such as missing scenarios, limited frequency band coverage, lack of spatial consistency with many associated defects to it, and inappropriate cluster definition for higher frequency bands and large antenna arrays. For example, large arrays may provide sufficient aperture to resolve individual sub-paths of clusters, which necessitates a new careful modeling of intra-cluster characteristics. The 5G channel model of 3GPP specified in [3GP17b] does still not fill all the gaps or meet all the requirements. As [JS16] summarizes, a significant research effort is needed to address all problems.

In addition to communications, radio can also be used for other purposes, such as positioning and radar. They are both applications that would require extension of the current GSCMs. The peculiarities and modeling requirements of vehicular multipath channel for radar are discussed in [JY19]. Intended and interfering path types in both urban and highway scenarios are thoroughly described. The automotive radar channel model must capture the physical locations of the radar, targets to detect and possible wave reflection and scattering objects. Thus, [JY19] proposes to study a hybrid of deterministic and stochastic model for radar evaluations.

2.2.2.3 Antenna modeling is a part of channel modeling

A realistic modeling of antennas, both individual elements and arrays, has been essential since the advent of MIMO communications and it is even more important now with 5G where antenna arrays may be very large (even massive) and their angular resolution very high. Antenna modeling, with polarimetric angular radiation patters, is a strength of GSCMs and deterministic channel models. Antenna patterns can be imported from antenna measurements or electromagnetic simulation tools. Alternatively patterns can be specified by mathematical functions. Arrays are specified in standard GSCMs by individual element patterns and array geometries, i.e. relative positions of elements within the array. The modeling principle also supports definition of antenna elements within an array into a common phase reference. In this case the array geometry is redundant as its effect is included in phases of element patterns.

2.2.2.3.1 Rotating antennas is a not trivial task

There is often a need to turn and tilt antennas to other orientations than the original measured/simulated orientation. The operation is not trivial, as the radiation pattern has vector coefficients with, e.g., E_ϕ and E_θ unit vectors. [ZMK18] gives a practical procedural description of rotating a complex polarimetric antenna radiation pattern to any direction specified by an arbitrary unit vector. First the antenna pattern, specified presumably in the spherical coordinate system, is transformed to the Cartesian coordinates. Target rotations along the three axes of Cartesian coordinate system are specified by 3×3 rotation matrices and the actual rotation operation is the matrix product of the rotation matrix and the radiation pattern in Cartesian coordinates. Fi-

nally the rotated pattern is transformed back to spherical coordinates. The power normalization has to be considered carefully when transforming between coordinate systems and performing the rotation matrix product.

2.2.2.4 Generality of models

Another benefit of GSCMs is their capability to construct different propagation environments and radio channel conditions boundlessly. A new "environment" is constructed each time a new model parametrization is drawn from probability distributions that specify a canonical propagation scenario. On the other hand, deterministic channel models, discussed in Section 2.2.1, are usually site specific. They are assumed to be capable of constructing only limited statistical variability of propagation conditions. Validity of this assumption is briefly touched in [HK16], where a simulation study using a map-based model [KLMLa17] is performed. The map-based channel model is a simplified site-specific model that also contains a random element, as originally proposed in [MSA02]. The question is, whether a deterministic model can provide similar statistical variations of propagation parameters as a GSCM specifies. Strictly and mathematically the answer is yes, if the map area is large and versatile enough and sufficiently many transceiver locations can be deployed. In [HK16] the so-called Madrid grid is 400×550 meters and 24 Transmitter (Tx) (Base Station (BS)) sites and 501 Receiver (Rx) (User Equipment (UE)) sites were simulated and resulting delay spreads, azimuth (UE side) spreads and Ricean K-factors were collected to derive empirical probability distributions. Rather high variation of parameters was found and the "satisfactory generality" of the map-based model was concluded. This is an interesting insight as deterministic channel model have become more attractive, and further work is required to determine to which extent this can be generalized to other scenarios and situations.

A related study is performed in [SR19] where a ray tracing, map-based, and a hybrid channel model output parameters and their second moments are compared. The first two models characterized specific streets of the city of Beijing and the hybrid model is built on identified dominant propagation paths of the map-based model. The hybrid model adds wave scattering points around those of dominant propagation paths randomly using an angular spread specific to the interaction type. A significant variation of resulting propagation parameters along the modeled route was observed.

2.2.2.5 Deterministic modeling of ground reflections in mmWave cellular GSCM

A characteristic of the mmWave band radio channel in cellular scenarios is the dominance of specular reflections over other propagation interaction mechanisms. In particular the ground reflection has a strong effect on the received power level. This is illustrated by a 60 GHz channel measurement in Fig. 2.16 [PWK+15]. The measured channel gain shows a similar dependence over link distance, up to 25 dB, as the well known two-ray model of Line of Sight (LOS) and ground reflection. The mean of both curves would follow approximately the free space path loss, but with a significant fluctuation that depends on the link distance and antenna heights. As a

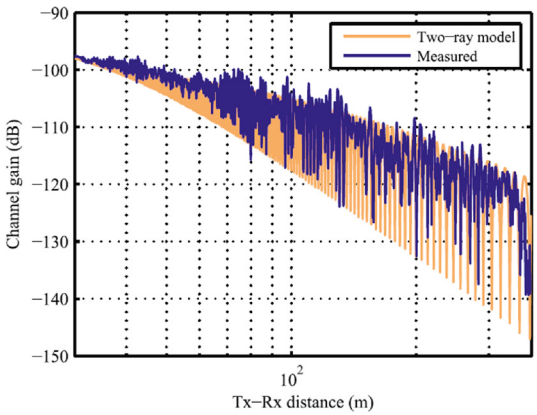

FIGURE 2.16

Comparison of measured channel gain vs. the two-ray model of LOS and ground reflection [PWK+15].

consequence, it is essential to model the ground reflection as a deterministic geometry dependent component, not as a random path. Introducing this deterministic component improves spatial consistency of a GSCM. A detailed derivation of a ground reflection model is given in [PWK+15]. It is based on Fresnel reflection coefficient, deterministic path lengths, and material permittivity.

2.2.2.6 Probability of LOS and reflected paths is derived

A GSCM does not contain a map, but typically only transceiver locations and antenna heights in a Cartesian coordinate system. Consequently, the availability of the LOS path is typically drawn randomly based on a LOS probability function. Furthermore, GSCMs usually specify propagation parameter distributions and path loss models, which may differ substantially, for LOS and Non Line of Sight (NLOS) conditions. LOS probabilities as well as ground and single wall reflection probabilities are investigated by a simulation study in [SJG16]. The map-based model assuming the so-called Madrid grid map is used together with numerous random transceiver locations to determine the probabilities as a function of link distance. The four studied scenarios are mobile-to-mobile, urban macro and micro, and urban micro open square. The study derives empirical cumulative distribution functions based on the binary existence of the LOS or reflected paths. Some interesting remarks were made, partly with respect to the LOS probabilities of the 3GPP model [36.15]. Firstly, the ground reflection does not always follow the LOS path, since in macro scenarios the roof-edge may block the path. Secondly, in the open square scenario the current 3GPP LOS probability formula is inadequate and needs a simple modification. Thirdly, most of the time the probability of finding a single wall reflection is higher than finding the LOS or ground reflected paths. Further simulations with various city layouts are planned as future work.

2.2.2.7 Map assisted LOS determination

The same question of LOS probability, but now with the aim of spatial consistency is discussed in [Ale17b] where a spatial consistent LOS/NLOS state model for GSCMs is proposed. The spatially-consistent model provides areas in a Cartesian coordinate system that indicates whether a UE connected to a particular BS site has LOS. The proposed model is map-assisted and accounts for building heights and densities, dividing the map area to two categories depending on this building information. This work is extended to support for time-varying MIMO channels in [ACS18]. There the so-called large scale parameters are generated on a map according to the determined LOS/NLOS regions. Cluster centers (wave interaction points) are drawn randomly in the coordinate system. Overall, the proposal aims to combine elements from stochastic and map-based models.

2.2.2.8 GSCM for non-terrestrial networks is under development

Though many satellite, atmospheric, and satellite-to-ground channel models have been defined in the past decades, 3GPP has not specified a MIMO channel model for Non-Terrestrial Networks (NTN). NTNs contain communications to ground level from different satellite orbits and from so-called High Altitude Platform Stations (HAPS), operating typically in altitudes between 8 and 50 km. A unified channel model concept for both terrestrial and NTN is described in [JBGS18]. The proposal is to keep the [3GP17b] model for fast fading and to extend it by adding components for long propagation delays, high Doppler shifts, and atmospheric effects like molecular absorption and scintillation. This is sketched in Fig. 2.17. The elevation angle is an essential parameter determining characteristics of MPCs and also molecular absorption. Large scale parameters, i.e., delay and angular spreads are extracted from ray-tracing simulations for various elevation angles and reported in [JBGS18]. These parameters are directly applicable to the GSCM of [3GP17b].

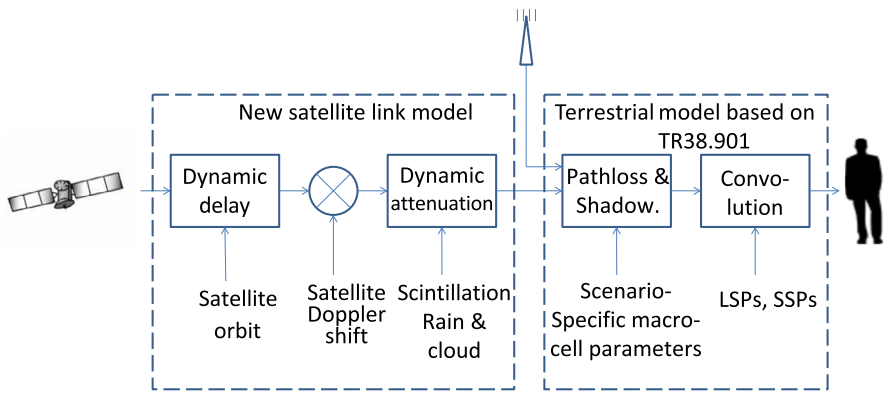

FIGURE 2.17

Block diagram of concatenated satellite and terrestrial models [JBGS18].

2.2.2.9 Clustered delay line model is a degenerated reference model of GSCM

Along the course of standardized GSCMs, there has been a need for limited randomness models, typically for uses like calibration of different implementation of the same channel model. For that purpose the concept of Clustered Delay Line (CDL) model was original developed. In CDL models the stochastic parameters are fixed and each time statistically identical MIMO fading channels are generated. This target is not reached, however, with the current procedure of, e.g., [3GP17b] in all conditions, as described in [KKH18]. Namely, with non-isotropic antennas and varying wave polarizations, the power angular distribution may vary because of a few random components of CDL. This may cause pessimistic performances in Time Division Duplex (TDD) communication simulations and prevent comparison of different uses of CDL models in link performance evaluations; [KKH18] proposes a few simple and non-disruptive modifications to guarantee wide sense stationarity over the ensemble of model runs by removing the unwanted randomness.

2.2.2.10 Analytical SINR model in urban microcells is derived by considering environmental randomness in BS deployment

Stochastic geometry has gained interest in many applications; [WVO17] is using it for urban coverage estimation by introducing random environments and physically motivated shadowing models. A Manhattan grid with straight perpendicular streets together with randomly drawn BS sites is generated by two one-dimensional homogeneous Poisson Point Processes. A UE is located in the center of the coordinate system. Different path types can be easily identified; LOS path is modeled with the free space path loss, penetration loss depends on the number of walls, and corner diffracted paths are modeled with the Berg's recursive model [Ber95]. For the case of identical transmit powers of BS, a mathematically tractable model has been determined for the Signal-to-Interference-plus-Noise Ratio (SINR) experienced by the UE and consequently for the coverage probability.

2.2.3 Enhanced COST2100 model

The COST 2100 MIMO channel model [LOP+12] is a spatially consistent GSCM that uses the concepts of clusters and Visibility Regions (VRs) to capture correlation effects and control the extent of scatterers' contribution to the channel. The model is a measurement based model for frequencies below 6 GHz and has been extended to cope with massive MIMO channels [FLET20,GFD+15] to cover the specific properties of the radio channel that are important in such systems during the COST-IRACON action. A MATLAB® implementation of the extension as well as the legacy model is freely available [IRA18]. Transmit arrays, receive arrays, clusters and scatterers are placed in a simulation area according to the routes of interest and prescribed distributions. It is the positions of the scatterers in the map, rather than directions and angles, that form the basis for the calculations of the contribution of each MPC to the total received signal. The model is inherently spatially consistent

and capable of handling spherical wavefronts. The COST IRACON massive MIMO extension [FLET20] includes:

1. introduction of VR at the BS,
2. introduction of a gain function of individual MPCs,
3. generalization to full 3D geometries, and
4. full parameterization in indoor and outdoor scenarios at 2.6 GHz.

2.2.3.1 Visibility regions on base station sides

The introduction of VR at the BS is motivated by the fact that when the antenna arrays get physically larger, the radio channel cannot be seen as WSS over the array, but the statistics change over the array. Measurements in [PT12,GTE13] have shown that clusters appear and disappear along physically large arrays, which means that both the angular spread as well as the delay spread change over the array. This effect is typically not captured by conventional MIMO channel models, but could be important both when determining beamforming strategies as well as for realistic performance assessment and system simulations.

The appearance and disappearance of new clusters are modeled by a Poisson process along the array with an intensity of λ new or dead clusters per meter. For an array spanning the interval x_1 to x_2, the number of observed BS VRs (and clusters) is thus given by

$$N(x_1, x_2) \in Poi(\lambda \cdot (x_2 - x_1) + \lambda \cdot E(Y)), \tag{2.1}$$

where $E(Y)$ is the scenario dependent mean length of the visibility area at the BS, further details are described in [FLET20]. Fig. 2.18 shows an example from a measurement with a 7.5 m long uniform linear array in a LOS scenario at 2.6 GHz together with the modeled parameters. Over the whole array the median value of clusters seen is 23, but not all of them are visible at the same spot of the array. Six of the clusters can in median be seen over the whole array, and 17 clusters are in the median observable only at some parts of the array.

2.2.3.2 Gain functions of multipath components

The gain function of individual MPCs is introduced as measurements have shown [LLO+19] that individual MPCs have a limited lifetime within the cluster when the UE moves and that different MPCs of a cluster are active at different locations within a VR as illustrated in Fig. 2.19. To model this phenomenon, a gain function, with a Gaussian shape in the spatial domain and with its peak randomly located within the cluster, is connected to each MPC. These gain functions are used as weighting functions for the MPCs so that depending on where the UE is located in the VR, it sees different weighted combinations of them. This retains the spatial consistency of the model at the same time as it captures the fine details of the channel that are important for realistic assessment of user separability, especially when they are closely located, and for more advanced forms of radio based localization and navigation such as multipath aided navigation and tracking.

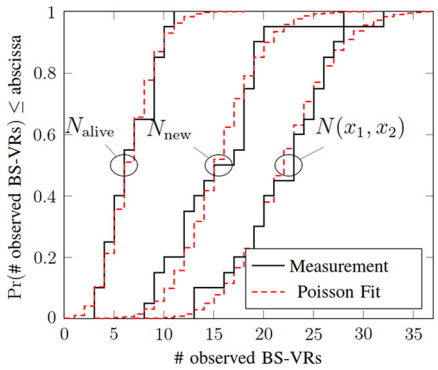

FIGURE 2.18

Observed visibility regions over a physically large array. $N(x_1, x_2)$ is the number of observed visibility regions (or clusters), N_{new} is the number of appearing visibility regions and N_{alive} is the number of already existing visibility regions [FLET20].

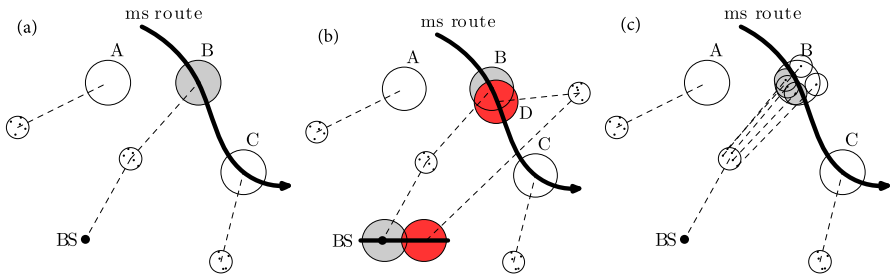

FIGURE 2.19

A MS moves in and out of various VRs, here named A, B, C, and D. (a) When the MS enters a VR, the associated cluster becomes active (VR B). (b) When a physically large array is used, different parts can observe different sets of clusters. (c) The relative gain of individual MPCs is controlled by MPC VRs, one for each MPC.

The lifetime, or rather the length of the spatial region within the VR where an MPC has a somewhat significant contribution to the observed impulse response, is a random parameter determining the radius of the MPC VR and the corresponding width of the gain function. Some MPCs have long lifetimes whereas the majority of MPCs actually can be observed only in a limited area and thus have short lifetimes and small MPC VRs. Measurements in an indoor sports hall [LLO+19] show that MPC lifetimes are best described by a log-normal distribution for the radii of the MPC VR. To have a smooth onset of the activation of a specific MPC we model the relative contribution of each MPC to the total channel gain by means of the gain

function [GFD+15,GERT15]. A Gaussian profile

$$g_{\mathrm{MPC},l}(\vec{r}_{\mathrm{MS}}) = \exp\left(-\frac{(\vec{r}_{\mathrm{MS}} - \vec{r}_{g,l})^2}{2\sigma_{g,l}^2}\right) \tag{2.2}$$

multiplies the complex amplitude of each MPC. Thus, the weight of a particular MPC depends on the Euclidean distance between the UE position $\vec{r}_{\mathrm{MS}}$ and the center of the l-th MPC VR $\vec{r}_{g,l}$. The centers of the MPC VRs are uniformly distributed within the cluster VR. The lifetime of the MPC is in this way determined by the width of the Gaussian profile. This width is controlled by $\sigma_{g,l}$ and is modeled as a log-normal parameter [FLET20].

2.2.3.3 Support of three-dimensional geometry

The need for generalization to 3D geometries and support for polarimetric channels comes naturally with the more advanced antenna arrangements used for massive MIMO. The BSs, UEs, scatterer locations and VRs can all be described by their 3D coordinates in the simulation area and any array geometry is supported as the individual antenna locations also are described by their individual coordinates. Antenna gain patterns are included at an individual antenna level, and can either be in the form of measured antenna responses, simulated responses or set as an arbitrary mathematical function (including the case of omnidirectional antenna responses). The COST family of channel models inherently captures spherical wave front effects as scatterer locations are defined by their coordinates in the simulation area rather than their directions with respect to BS and UE antennas. As the model output is the transfer function matrix (or equivalently, the impulse response matrix after inverse Fourier transform) between BS antenna array and UE antennas, any kind of digital, analog or hybrid beamforming can be analyzed.

2.2.3.4 Available parameters of the model

Finally, the COST IRACON massive MIMO extension is parameterized and validated based on measurements for physically large outdoor arrays at 2.6 GHz in LOS and NLOS, and with indoor and outdoor measurements for closely located users at 2.6 GHz using a physically smaller circular array. The list of parameters can be found in Table 2.1, and a detailed model description can be found in [FLET20].

2.2.4 Reference ITU-R path loss models

A number of ITU recommendations address path loss models depending on the environment, frequency band and BS-UE range. These include

- Recommendation ITU-R P.1411 [Rec17b] for short range outdoor scenarios up to 1 km and in the frequency range of 300 MHz to 100 GHz;
- Recommendation ITU-R P.1238 [Rec17a] for indoor scenarios in the frequency range of 300 MHz to 100 GHz;

Table 2.1 Parameterization of the COST 2100 model extension for closely-located users with physically-large arrays and CLA at 2.6 GHz [FLET20].

Parameter	Outdoor (NLOS)	Indoor (LOS)
Length of BS-VRs, L_{BS} [m]	3.2	-
Slope of BS-VR gain, μ_{BS} [dB/m]	0	-
Slope of BS-VR gain, σ_{BS} [dB/m]	0.9	-
MPC gain function, $\mu_{R_{\mathrm{MPC}}}$ [dB]	-	−19.8
MPC gain function, $\sigma_{R_{\mathrm{MPC}}}$ [dB]	-	10.1
Average number of visible far clusters, N_C	$2.9 \times (L_{\mathrm{BS}} + L)$	15
Radius of the cluster visibility region, R_C [m]	10	5
Radius of cluster transition region, T_C [m]	2	0.5
Number of MPCs per cluster, N_{MPC}	31	1000
Cluster power decay factor, k_τ [dB/μs]	43	31
Cluster cut-off delay, τ_{B} [μs]	0.91	0.25
Cluster shadowing, σ_S [dB]	7.6	2.7
Cluster delay spread, m_τ [μs]	0.14	0.005
Cluster delay spread, S_τ [dB]	2.85	1.5
Cluster angular spread in azimuth (at BS), $m_{\psi_{\mathrm{BS}}}$ [deg]	7.0	4.6
Cluster angular spread in azimuth (at BS), $S_{\psi_{\mathrm{BS}}}$ [dB]	2.4	2.1
Cluster angular spread in elevation (at BS), $m_{\theta_{\mathrm{BS}}}$ [deg]	0	3.7
Cluster angular spread in elevation (at BS), $S_{\theta_{\mathrm{BS}}}$ [dB]	0	2.6
Cluster angular spread in azimuth (at MS), $m_{\psi_{\mathrm{MS}}}$ [deg]	19	3.6
Cluster angular spread in azimuth (at MS), $S_{\psi_{\mathrm{MS}}}$ [dB]	2.0	2.1
Cluster angular spread in elevation (at MS), $m_{\theta_{\mathrm{MS}}}$ [deg]	0	0.7
Cluster angular spread in elevation (at MS), $S_{\theta_{\mathrm{MS}}}$ [dB]	0	3.6
Cluster spread cross-correlation,		
$\rho_{\sigma_S \tau}$	−0.09	−0.45
$\rho_{\sigma_S \psi_{\mathrm{BS}}}$	0.04	−0.56
$\rho_{\sigma_S \theta_{\mathrm{BS}}}$	0	−0.50
$\rho_{\tau \psi_{\mathrm{BS}}}$	0.42	0.70
$\rho_{\tau \theta_{\mathrm{BS}}}$	0	0.34
$\rho_{\psi_{\mathrm{BS}} \theta_{\mathrm{BS}}}$	0	0.50
Radius of LOS visibility region, R_L [m]	-	30
Radius of LOS transition region, T_L [m]	-	0
LOS power factor, $\mu_{K_{\mathrm{LOS}}}$ [dB]	-	−5.2
LOS power factor, $\sigma_{K_{\mathrm{LOS}}}$ [dB]	-	2.9
XPR, μ_{XPR} [dB]	0	9
XPR, σ_{XPR} [dB]	0	3

- Recommendation ITU-R P.2108 [Rec17c] gives models for the prediction of clutter loss;
- Recommendation ITU-R P.2109 [Rec17d] is for building entry loss;

- Recommendation ITU-R P.1546 which covers point-to-area path loss predictions for terrestrial services in the frequency range 30 MHz to 3000 MHz;
- Recommendation ITU-R P.528 on the prediction of point-to-area path loss for the aeronautical mobile service for the frequency range 125 MHz to 15.5 GHz and distance range up to 1800 km;
- Recommendation ITU-R P.617 for the prediction of point-to-point (P-P) path loss for trans-horizon radio-relay systems for the frequency range above 30 MHz and for distances from 100 to 1000 km;
- Recommendation ITU-R P.530 for the prediction of P-P path loss for terrestrial line-of-sight systems; and
- Recommendation ITU-R P.2001 [Rec19] which provides a wide-range of terrestrial propagation models for the frequency range 30 MHz to 50 GHz including both fading and link enhancement statistics.

In this section we review the ITU path loss models for outdoor short range, indoor environments, clutter loss and building entry loss, which cover the high frequency bands including the millimeter wave bands proposed for 5G cellular networks.

2.2.4.1 Indoor environments

Recommendation ITU-R P.1238-9 [Rec17a] gives transmission loss models for indoor environments which assume that the BS and the UE are located inside the same building. It provides two models: a site-general model and a site specific model.

The site-general model is given by

$$L_{\text{total}} = L(d_o) + N \log_{10}\left(\frac{d}{d_o}\right) + L_f(n) \text{ dB}, \tag{2.3}$$

where N is a distance power loss coefficient, f is frequency (MHz), d is a separation distance (m) between BS and UE where $d > 1$ m, d_o is a reference distance (m), $L(d_o)$ is the path loss at d_o (dB) for a reference distance d_o at 1 m, and assuming free space propagation $L(d_o) = 20\log_{10} f - 28$ where f is in MHz; L_f is the floor penetration loss factor (dB) and finally n is the number of floors between BS and UE ($n \geq 0$), with $L_f = 0$ dB for $n = 0$.

The recommendation provides typical parameters, based on various measurement results from 0.8 GHz to 70 GHz in residential, office, commercial, factory and corridor environments with the office environment being the most characterized across the bands, and at 300 GHz for a data center. Tables 2 and 3 in [Rec17a] give the values of the coefficient N based on $d_o = 1$ m, and floor penetration loss factors, L_f (dB), respectively. The shadow fading statistics, standard deviation in dB, is given in Table 4 of [Rec17a].

The site specific model refers to the estimation of path loss or field strength, based on the uniform theory of diffraction and RT techniques which require detailed information of the building structure. It recommends including reflected and diffracted rays to improve the accuracy of the path loss prediction.

2.2.4.2 Outdoor short range environment

Recommendation ITU-R P.1411-9 [Rec17b] also provides site-specific and site-general propagation models across various frequency bands for LOS and NLOS scenarios. It also classifies the environments as urban very high rise, urban high rise, urban low rise/suburban, residential and rural. It also defines three cell types: micro-cell for ranges between 0.05 to 1 km, dense urban micro-cell for ranges between 0.05 to 0.5 km and pico-cells for ranges up to 50 m where the station is mounted below rooftop.

The site-general model applies to two scenarios where the two terminals, i.e., Tx and Rx, are below rooftop heights and where one terminal is above the rooftop height and the second terminal is below the rooftop. The site general model for both scenarios is given by

$$PL(d, f) = L(d_o) + 10\alpha \log_{10}(d) + \beta + 10\gamma \log_{10}(f) + N(0, \sigma) \text{ dB}, \qquad (2.4)$$

where d is a 3D direct distance between the transmitting and receiving stations (m); f is the operating frequency (GHz); α is a coefficient associated with the increase of the path loss with distance; β is a coefficient associated with the offset value of the path loss; γ is a coefficient associated with the increase of the path loss with frequency; and finally, $N(0, \sigma)$ is a zero mean Gaussian random variable with standard deviation σ (dB).

This model provides coefficients which cover a wide frequency range. Table 4 in the recommendation provides the coefficients of the model for below the rooftop scenario for urban high rise, urban low rise and suburban for LOS and NLOS for up to 73 GHz and from 5 m to 715 m depending on the environment. Frequencies are covered depending on the environment and with ranges varying. Table 8 in the recommendation provides the coefficients for above the rooftop scenario for urban and suburban environments up to 73 GHz.

The recommendation also provides two site-specific models for LOS and NLOS scenarios where in the LOS case, it adopts a dual slope model with a breakpoint up to 15 GHz. For the millimeter wave band a single slope model is recommended since the breakpoint will occur beyond the expected range of the cell. In this case the path loss model is given by

$$L_{\text{LoS}} = L_0 + 10n \log_{10}\left(\frac{d}{d_0}\right) + L_{\text{gas}} + L_{\text{rain}} \text{ dB}, \qquad (2.5)$$

where L_{gas} and L_{rain}, are attenuation by atmospheric gases and by rain which can be calculated from Recommendation ITU-R P.676 and Recommendation ITU-R P.530, respectively. Typical values of the path loss coefficient from LOS measurements with directional antennas are in the range of 1.90 to 2.21.

2.2.4.3 Clutter loss

Clutter refers to objects, such as buildings and vegetation, which are on the surface of the earth but not actually terrain. Clutter loss models in Recommendation ITU-R

P.2108 [Rec17c] are statistical, where clutter loss is defined as the difference in the transmission loss with and without the presence of clutter. It is therefore, the difference between free space loss and the loss in the presence of clutter.

The statistical clutter loss model for terrestrial links can be applied for urban and suburban environments. It gives the clutter loss L_{ctt}, not exceeded for p % of locations for the terrestrial-to-terrestrial link by the following set of equations:

$$L_{\text{ctt}} = -5\log(10^{-0.2L_l} + 10^{-0.2L_s}) - 6Q^{-1}(p/100)\ \text{dB}, \tag{2.6}$$

where $Q^{-1}(p/100)$ is the inverse complementary normal distribution function, and

$$L_l = 23.5 + 9.6\log(f)\ \text{dB}, \tag{2.7}$$

$$L_s = 32.98 + 23.9\log(d) + 3\log(f)\ \text{dB}, \tag{2.8}$$

where d is the 3D link distance.

2.2.4.4 Building entry loss

The building entry loss model in Recommendation ITU-R P.2109-0 [Rec17d] is based on measurement data collated in Report ITU-R P.2346 in the range from 80 MHz to 73 GHz. The model is given for two types of buildings: traditional and thermally efficient; where in the case of modern, thermally-efficient buildings (metalized glass, foil-backed panels) building entry loss is generally significantly higher than for "traditional" buildings without such materials. The model therefore gives predictions for these two cases where it is assumed that the indoor antenna is omnidirectional.

The building entry loss distribution is given by a combination of two log-normal distributions. The building entry loss not exceeded for the probability, P, is given by

$$L_{\text{BEL}}(P) = 10\log(10^{0.1C(P)} + 10^{0.1B(P)} + 10^{0.1C})\ \text{dB}, \tag{2.9}$$

where:

$$A(P) = F^{-1}(P)\sigma_1 + \mu_1, \tag{2.10}$$

$$B(P) = F^{-1}(P)\sigma_2 + \mu_2, \tag{2.11}$$

$$C = -3.0, \tag{2.12}$$

$$\mu_1 = L_h + L_e, \tag{2.13}$$

$$\mu_2 = w + x\log(f), \tag{2.14}$$

$$\sigma_1 = u + v\log(f), \tag{2.15}$$

$$\sigma_2 = y + z\log(f), \tag{2.16}$$

where $L_h = r + s\log(f) + t(\log(f))^2$ is the median loss for horizontal link paths and $L_e = 0.212|\theta|$ is the correction for elevation angle of the link path at the building facade; f is the frequency (GHz); θ is the elevation angle of the path at the building facade (degrees); P is the probability that the loss is not exceeded ($0.0 < P < 1.0$); finally, $F^{-1}(P)$ is the inverse cumulative normal distribution as a function of probability.

2.2.5 Models for dense multipath components

Dense multipath components (DMCs) represent the part of the radio propagation channel that can not be characterized by a superresolution of distinct plane waves [PSH+15]. In other words, the continuous power spectrum representation is more appropriate for the DMC. In typical indoor scenarios, DMC may include 1) DiS originated from rough surfaces whose height deviation is greater than the wavelength of the carrier frequency, and 2) the reverberation of radiated energy due to a multitude of specular components, e.g. multiple reflections and multiple scatterings, which typically occurs in a closed or partially-closed cavity.

While Section 2.2.1.2.3 covers microscopic modeling of DiS, there also exists macroscopic modeling of the DMC. It can be modeled empirically and holistically as fitting to the residue of the measured channel after excluding Specular Multipath Component (SMC), as detailed in Section 2.3. Empirical evidence of significant DMC is found in a number of papers in literature. It contributes to more than 30% of the total channel power for LOS scenario at 11 GHz in indoor scenarios, and depends on angle and polarization for a frequency range from 3 to 28 GHz [VBJO17,SiTK17,HST+18,SHF+19]. DMC contributes up to 70% of the total channel power at 3 GHz in an industrial environment [TGL+14] and up to 40% and 86% in LOS and NLOS indoor channels [PSH+15]. Polarimetric characterization of DMC is also of great interests, as discussed for an industrial hall at 1.3 GHz and an urban site at 4.5 GHz [GTJ+15,LST+07]. Steinböck et al. [SPF+13] defined a term reverberation ratio to model the DMC contribution to the total channel power that depends on the distance between Tx and Rx antennas.

Despite the potential large power contribution to the total channel power and the impact on the polarization and angular characteristics of multipath channels, DMC have not yet been considered explicitly in standard channel models, except for the COST2100 model detailed in Section 2.2.3. Therefore, measurements, characterization and modeling of DMC for various application scenarios are necessary. In particular, when DMC dictates the total channel power, the comprehensive modeling of DMC in temporal-spatial-frequency domain is crucial for studies of wideband and multiple-antenna radio systems [MGO18,KWG+18].

Statistical and macroscopic modeling of DMC looks at reverberation of electromagnetic fields inside a confined space as in [Ped18,MPG+19b,AP18b,AP18a, Ped19,APB18]. Multipaths due to DiS typically have longer delays than those of SMC and hence forming a "tail" in the power delay profile (PDP) of channels. The tail can be described as an exponentially decaying function with fluctuations; an exemplary indoor PDP is shown in Fig. 2.20. As the DMC represents reverberation of energy, multiple bounce specular reflections or multiple bounce DiS describe the phenomenon.

2.2.5.1 Analysis of diffuse scattering

One of the challenges in proper modeling of DiS is to obtain its observations either from measurements or computation. The latter usually allows more rigorous analysis than measurements as different surface samples can be individually considered. DiS

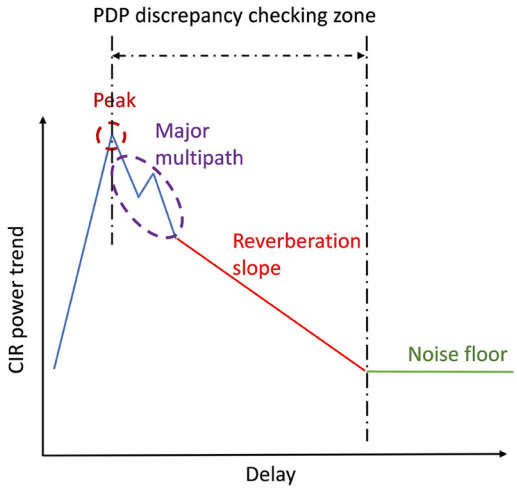

FIGURE 2.20

Typical shape of indoor PDP consisting of SMC, a slope representing DMC and noise floor [MPG+19b]. CIR indicates Channel Impulse Response.

from rough surfaces can be computed, for example, by Physical Optics (PO) introduced in Section 2.2.1.4. The surface roughness (or equivalently irregularity) can be statistically described as an Effective Roughness (ER) model using, e.g., a correlated Gaussian process [Ves91], while the same can also be measured for existing surfaces as point clouds as discussed in Section 2.2.1.3 [JHK16]. Miao et al. [MGO18] investigated the spatial coherence of DiS multipath by applying PO to ER model of a surface. In PO, the rough surface is first divided into triangles whose side length is in the order of 0.1 times the wavelength. The EM field on each triangle is then approximated to equivalent PO current to derive the Channel Transfer Function (CTF). Different from PO, the side length of facet in ER is determined by the far-field distance from Tx and Rx. They derived the spatial correlation of DiS multipath from a rough wall using its ER model. With a fixed Tx antenna, phase correlation of DiS multipaths over Rx antenna locations decreases. The speed of decrease depends on the surface roughness and the relative position between Rx and the wall.

The work by Kulmer et al. [KWG+18] showed that DiS due to rough surfaces can have negative impacts on radio localization accuracy. DiS was generated in their GSCM using the ER models that reflect dielectric properties and locations of a rough surface. The ER models clearly impacted the shape of angular power spectrum and Power Delay Profile (PDP) of channels and hence the radio localization performance. Dense Multipath Component (DMC) behaves like an added Gaussian non-zero-mean noise to SMCs that are used for localization, resulting in biased angular and delay estimates of SMCs.

2.2.5.2 Modeling reverberation by propagation graphs

Propagation graph (PG) [PSF12,PSF14] is a promising approach to model the diffuse "tail" of a PDP due to reverberation of electromagnetic fields in a confined space. An exemplary PG is illustrated in Fig. 2.21, where the vertices represent the transmitters, the receivers and the scatterers presenting in the propagation environment. The edges model wave propagation between vertices including time delay, leading to time-dispersion of the channel. The surface roughness of objects in a propagation environment may impact the choice of the vertices in PG models [TEVY16,MPG+19b]. The major merit of PG modeling of DiS is that it yields a closed-form solution of a transfer function even if infinite bounces of radio waves on objects in the environment are involved.

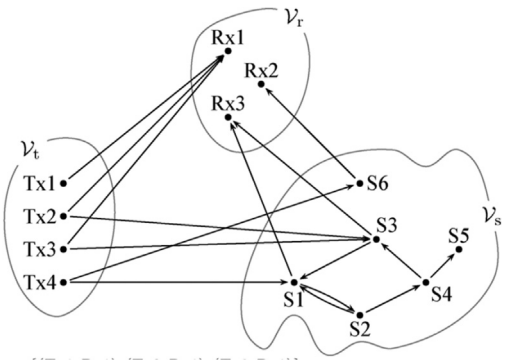

FIGURE 2.21

An exemplary propagation graph with four transmit vertices, three receive vertices, and six scatterer vertices [PSF12]. Signal propagation between vertices is represented by the edges and associated transfer matrices.

2.2.5.2.1 Application of propagation graph models to different scenarios

PG can be either stochastically or deterministically generated. It has been applied to different scenarios and has successfully predicted the radio channel properties, such as scenarios of in-room [PSF12], outdoor-to-indoor [PSF14], high speed railway [ZTS+15] and millimeter wave systems [CYTK17]. In addition, the hybrid of PG with RT has been applied to predict in-room scenarios [TEVY16,SGM+16]; RT and PG are capable of capturing major multipaths and diffuse reverberation "tail", respectively.

2.2.5.2.2 Extension of the propagation graph models

PG modeling of diffuse scattering and the calculation of reverberation components are extended to various application scenarios [Ped18,MPG+19b,AP18b,AP18a, Ped19,APB18]. For example, Adeogun and Pedersen [AP18b] have extended the original PG model in [PSF12] to be applicable to polarized multiple-antenna sys-

tems. The polarized PG model contains not only attenuation, delay, phase shifts, but also depolarization effects of wave propagation, scattering and antenna effects. The model was applied to predict the dual-polarized indoor MIMO channel in a cuboid. The simulation results showed that the diffuse reverberation "tail" of PDP of co- and cross-polarized channels has almost the same decay rate. The model is further extended to relate the powers of co- and cross-polarized signal components and their ratio with the number of scatterers, probability of scatterer visibility, reflection gain and polarization coupling parameters [AP18a].

Miao et al. [MPG+19b] show the use of PG for modeling DiS in room-to-room scenarios with the help of RT. The PG vertices were obtained in each room separately by RT with the assumption that Rx (or Tx) virtually locates on the surface of the separating wall between two rooms. The rays transmitted from one room to the other through the separating wall are calculated by Snell's law. Placing vertices of PG in each room separately allows simplest modeling of DiS multipaths in the scenario, based on two assumptions: 1) no propagation from the room containing Rx back to the room containing Tx and 2) RT applied separately to each room only involves propagation mechanisms of LOS and first order specular reflection.

2.2.5.2.3 Propagation graph of reduced complexity

DiS observed in PDPs results from waves bounced on surfaces many times. In the closed-form CTF produced by PGs, there is a fraction of matrix inversion. The inversion represents the infinite interaction loops among scatterers, but may result in a heavy computation load with the increased number of scatterers and hence vertices. To cope with this problem, [APB18] has proposed an equivalent PG model of reduced complexity in computing the CTF when Tx and Rx are located in different rooms. A vector signal flow has been proposed for PG where rooms in the complex large environment are denoted as nodes and the propagation between rooms is as branches. The proposed equivalent model was shown to yield the same accuracy of prediction as the original PG model in [PSF12] but with much lower computational complexity.

2.2.5.2.4 Path arrival rate

Pedersen [Ped18,Ped19] has modeled the path arrival rate of a propagation channel when Tx and Rx equipped with directive antennas are in the same room. PG and the mirror source theory are used for the model. A notion of "mixing time" is defined as the onset of the diffuse reverberation "tail", and as the point in time where the arrival rate exceeds one component per transmit pulse. This definition was inspired by Eyring's empirical model of the reverberation time, which has been experimentally evaluated in [SPF+15].

2.2.5.2.5 Combination of propagation graph and geometry-based channel model

Finally, Vinogradov et al. [VBJO17] have modeled dynamic PDPs of room-to-room channels. The model is a physical-statistical combination of 1) room electromag-

netic theory for the deterministic components and of 2) GSCM with time-variant statistics for the stochastic components. The deterministic components are the major multipaths followed by an exponentially decaying slope in PDP, while the stochastic components represent large-scale variations such as shadowing and small-scale variations over time and delays. The work reported non-stationary fading of dynamic indoor channels across time and delays. Their variation has been characterized using the Rician K-factor and the t-location scale distribution parameters for small- and large-scale fading. A Hidden Markov model was used to describe the evolution of the small-scale fading statistics.

2.2.5.3 Experimental characterization of dense multipath components from channel measurements

Observations of DMC from real-world radio channel sounding serve as a basis for developing its realistic models [VBJO17,SiTK17,HST+18,SHF+19,D'E19b]. In practice, DMC can be obtained as residue of measured channels after subtracting SMC.

2.2.5.3.1 Directional and polarimetric characteristics

Saito et al. [SiTK17] have characterized the DMC from the indoor LOS MIMO measurement at 11 GHz band with 400 MHz bandwidth. Statistics of DMC over frequency, angular and polarization domains were estimated jointly with a set of parameters for SMC as detailed in Section 2.3. Estimated DMC has shown directional and polarization dependence. The DMC occupies up to 30% of total channel power according to their measurements. In addition, with the decrease of the room size, the angular spreads of DMC increase, and their diffuse "tails" last longer over the delay, owing to stronger reverberation of energy inside the room. A similar analysis has also been reported by Hanssens et al. [HST+18] for measured radio channels at 11 GHz RF, where the Angular Power Spectrum (APS) of DMC is characterized by a multimodal Von Mises distribution better than the conventional unimodal one.

2.2.5.3.2 Dependence on carrier frequency

Measurements in IRACON also shed lights on frequency dependency of DMC. For example, D'Errico [D'E19b] characterized the DMC in a machinery room full of metallic objects for a band of 2 to 6 GHz. The DMC contributed to 11.8% and 24.7% of the total channel power in the measurements of LOS and NLOS scenarios, respectively. Their trend of exponentially decaying power in PDP, as the delay increases, was found to be similar across the band. Finally, Saito et al. [SHF+19] estimated DMC from MIMO measurements at 3, 10, and 28 GHz with the same bandwidth in a hall and a laboratory room. The work found that 1) the SMCs were similar in all investigated frequency bands and 2) the power and the angular spread of DMC tended to decrease as the carrier frequency increased.

2.3 Algorithms for estimation of radio channel parameters

Multipath component estimation for radio channels is limited by the finite apertures of the radio channel sounding equipment in the time, frequency, and spatial domains. Propagation paths that are low in power or are densely packed in the Doppler, delay, or angular domains can often not be fully resolved by state-of-the-art estimation algorithms. These paths are put under the umbrella of *dense multipath components (DMC)* and include diffusely scattered paths and low-power specular reflections. The DMC phases are considered to be random (i.e., are incoherent) and as such DMC can only be described by their power density in the Doppler, delay, and angular domains. This is in contrast to the high-power *specular multipath components (SMC)* that possess well-defined coherent phases.

2.3.1 Narrowband multipath component estimation

In classical narrowband multipath estimation, it is commonly assumed that the frequential and spatial domains are uncorrelated. Specifically, the change in wavelength (or equivalently, the electrical dimensions of the environment and the antenna arrays) over the considered bandwidth is deemed insignificant. This means that, in narrowband algorithms, we assume a constant wavelength while still allowing the frequency to vary across the bandwidth. We thus effectively separate space (wavelength) and frequency. This is an approximation to simplify calculations because, of course, frequency and wavelength are still always related by the speed of light. Moreover, the limited bandwidth implies that the reflectivity of the environment is constant and independent of frequency within that band. The narrowband assumption offers a few computational benefits to maximum-likelihood multipath estimation algorithms such as SAGE [FTH+99] and RiMAX [Ric05]. The separation of the frequential and spatial domains means that certain vectors or matrices in the signal model can be simply written as the Kronecker product of their one-dimensional versions across each of the multipath parameter domains separately. This so-called Kronecker separability is applied to the specular multipath steering vector and the dense multipath covariance matrix. The reduction in computational burden then stems from replacing the multidimensional parameter estimation with an iterative one-dimensional initialization and optimization scheme executed sequentially in each of the parameter domains.

2.3.1.1 An estimator for non-uniform angular dense multipath

Modern multipath estimation algorithms include DMC estimation based on mathematical models of the DMC power spectral densities with a priori unknown parameters. For example, the original RiMAX maximum-likelihood estimator assumes an exponentially decaying DMC power spectral density in the delay domain and a uniform distribution of DMC power in the angular domains [Ric05]. The uniform DMC angular spectrum in particular is hard to maintain in most realistic non-reverberating indoor and outdoor environments. For this reason, modifications to the mathematical model of the DMC angular spectrum have been proposed.

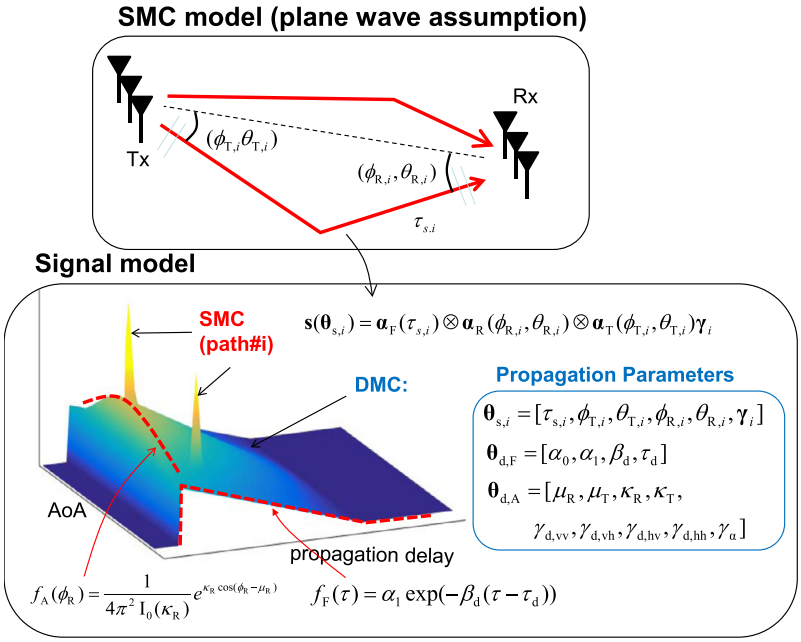

FIGURE 2.22

SMC and DMC data model for their parameter estimation [SiTK17].

A more fitting model for the DMC angular spectrum at transmitter and receiver is the Von Mises distribution, originally proposed in [RRK07]. The work in [SiTK17] incorporates a unimodal Von Mises model at transmitter and at receiver in the RiMAX estimator. Fig. 2.22 shows the used SMC and DMC signal model: the original RiMAX model is extended with a DMC propagation parameter vector $\boldsymbol{\theta}_{d,A}$ that includes the Von Mises mean angle and concentration parameters, and the power gains for the four polarization subchannels. Follow-up work in [HST+18] extends this to a multimodal Von Mises model that allows for multiple angular DMC clusters. The Von Mises extension to the RiMAX DMC data model has been validated with indoor radio channel sounding measurements at 11 GHz in both [SiTK17] and [HST+18]. The agreement between measurements and model was checked by comparing the distribution of the largest eigenvalues calculated from the measured MIMO channel matrix and from the channel matrix reconstructed with the model.

2.3.1.2 Specular multipath estimation from power spectra

The clustered MPCs are widely observed and used in channel characterization. To develop and evaluate advanced wireless systems at high frequency, directional scanning by highly directive antennas is the most popular method to obtain angular channel characteristics. However, it is often insufficient for ray-/cluster-level characterization and channel modeling because the angular resolution of the measured

data is actually limited by the angular sampling interval and antenna half power beamwidth for a given scanning angle range. In [KIU+20], the subgrid CLEAN algorithm was developed, which is a novel technique for high-resolution MPC extraction from the multi-dimensional power image, the so-called double-directional angular delay power spectrum. By applying the developed technique to measured data taken at 58.5 GHz in indoor environments assuming an in-room 5G hotspot access scenario, scattering processes are identified and multipath clusters are characterized: 8-12 clusters were observed within a dynamic range of approximately 40 dB as illustrated in Fig. 2.3.

2.3.1.3 A Bayesian estimator for specular and dense multipath

In [GLFW18], a sparse Bayesian learning (SBL) algorithm for the estimation of SMC and DMC parameters is introduced. The benefit of the SBL algorithm is that the number of SMC is assumed to be unknown and that number is estimated jointly with the SMC and DMC parameters. This is in contrast to maximum-likelihood or maximum a posteriori estimation for which the number of SMC is a priori fixed. The SBL algorithm is applied to both synthetic and measured data and returns SMC and DMC parameters with good accuracy. Importantly, the algorithm is shown able to detect SMC that have real physical representations in the radio environment and is good at suppressing specular artifacts that cannot be linked back to the environment.

2.3.2 Wideband multipath component estimation

2.3.2.1 A specular multipath estimator for ultra-wideband channels

A new multipath component estimator specifically developed for Ultra WideBand (UWB) radio channels is presented in [HTG+18]. The estimation framework is based on the RiMAX narrowband maximum-likelihood estimator [Ric05]. The ultrawide bandwidth is divided into sub-bands wherein the narrowband assumption can reasonably be expected to hold. Parameters of SMC and DMC are classified into parameters that are assumed to be constant over the full UWB bandwidth and parameters that are constant only in each sub-band. The parameters constant over the full bandwidth are specular multipath parameters that only depend on the geometry of the propagation environment, namely AoD, AoA, and ToA. These parameters are estimated by maximizing a *global* cost function that is a weighted sum of the narrowband RiMAX cost functions for each sub-band. The multipath parameters that are only constant in each sub-band are the complex amplitudes of the specular paths and the parameters of the theoretical power spectral densities associated with the dense multipath. These are estimated in each sub-band separately with the classical RiMAX estimator by maximizing *local* cost functions.

2.3.2.2 Joint delay and Doppler estimation for bistatic radar

In [DKS+19], a RiMAX-inspired maximum likelihood estimator is presented for the purpose of joint delay and Doppler estimation. The estimator is developed specifically for bistatic radar measurements that typically have transmitting sequences that

are relatively long. To take this into consideration, Doppler is modeled as a phase that changes linearly with time within one transmit symbol period. Delay and Doppler are estimated with an iterative maximum-likelihood scheme similar to RiMAX, i.e., a coarse grid-based initialization of both parameters followed by non-linear gradient-based optimization with the Gauss-Newton method. Model order selection is performed by discarding paths based on a criterion that compares the estimation error variance of path power to the estimated path power itself. The proposed estimator is applied to measurements with a carousel-type bistatic radar setup in a semi-anechoic chamber.

2.3.2.3 Comparison of multipath estimators for millimeter-wave channels

The work in [FJZP] presents frequency-swept millimeter-wave (28-30 GHz) indoor radio channel sounding measurements in both LOS and obstructed LOS scenarios. The goal of the work was to compare multipath estimates obtained from the channel sounding data with various multipath estimation algorithms. A single biconical antenna was used as Tx, while for the Rx a high-density virtual uniform circular array was created with a biconical antenna. Multipath component delay and AoA were estimated with these estimation algorithms: classical beamforming, frequency-invariant beamforming, space-alternating generalized expectation-maximization (SAGE) with either delay or AoA as the first search space, and maximum-likelihood estimation (MLE) with either a plane-wave or spherical wave signal model. The estimation output is compared with the true angular and delay distribution of multipath power, obtained by rotating an Rx horn antenna in all directions and measuring the channel impulse response. The comparative study of multipath estimation algorithms revealed a number of observations on their relative performance. For example, the multipath estimates of the MLE algorithm with spherical wavefronts are closest to the true angular and delay power distribution. This highlights the necessity of using the spherical-wave model for short-range millimeter-wave communication links.

2.3.3 Multipath component clustering

A large body of MIMO measurements has shown that MPCs occur in groups, also known as clusters, such that the MPCs within one group have similar characteristics, but have significantly different characteristics from the MPCs in other clusters. Separately characterizing the intra-cluster and inter-cluster properties can allow to significantly simplify channel models without major loss of accuracy. Therefore, many channel models have been proposed and developed based on the concept of clusters. Recently, automated algorithms of MPC clustering have gained popularity, but still suffer from the use of arbitrary thresholds and/or a priori assumption of the number of clusters [HAM+18].

2.3.3.1 Clustering based on kernel power density

In [HLA+17], a novel kernel power density (KPD) based algorithm is proposed for MPC clustering in MIMO channels, where the kernel density of MPCs is adopted to

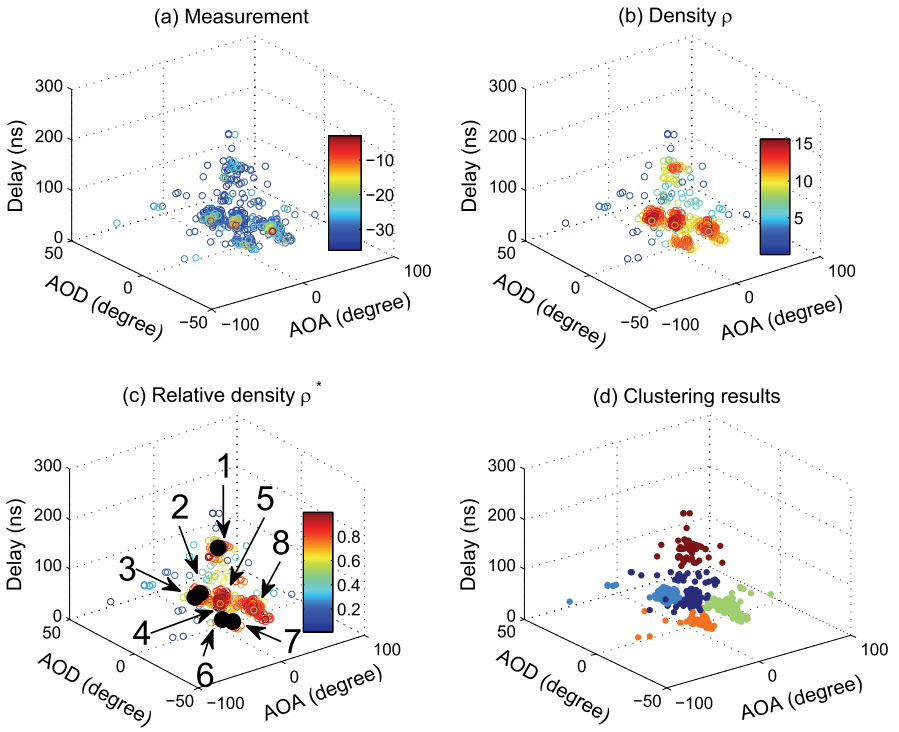

FIGURE 2.23

Illustration of KPD clustering using measured MPCs [HLA+17].

characterize the modeled behavior of MPCs. The KPD uses the kernel density and only considers the neighboring MPCs when computing the density. It also uses the relative density normalized within a local region, and a threshold is used to determine whether two clusters are density-reachable and are to be merged. To illustrate, an example is given in Fig. 2.23, where (a) shows the measured MPCs, (b) shows the estimated density of MPCs, (c) shows the estimated relative density, and (d) gives the final clustering results by using the KPD algorithm.

2.3.3.2 Sparsity-based clustering

The work in [HCA+16] introduces a novel algorithm to identify clusters in the time-delay domain. The intra- and inter-cluster power decay behavior is assumed to follow the well-known Saleh-Valenzuela (SV) double-exponential formulation [SV87]. The SV model parameters are estimated by fitting its mathematical model to the measured PDP in the least-squares sense, with an added weighted l_1-norm constraint. The l_1-norm constraint ensures that the intra-cluster power decay follows the exponential SV model and that the algorithm favors a small number of clusters (i.e., that the solution is sparse). A separate clustering enhancement approach is used, which

also forces the inter-cluster power decay to follow the expected SV model behavior. The result is an algorithm of fairly low computation complexity.

2.3.3.3 Clustering based on the Hough transform

In [CPYY18], a new MPC clustering algorithm is presented for vehicular channels. The algorithm is founded in the observation that, in time-variant power delay profiles $|h(t,\tau)|^2$ of vehicular channels, the power follows continuous curves with smoothly varying slopes. The MPC clustering detects and tracks these curves based on a modified Hough transform. The Hough transform is originally an image processing technique to find straight lines in black-and-white images [CPYY18]. The modified Hough transform for cluster detection includes a procedure to convert time-variant power delay profiles to black-and-white images, the removal of clutter points that are not part of a cluster of significant lifetime, and cluster tracking accounting for the smooth change of the cluster velocity relative to the receiver motion.

2.3.4 Large-scale parameter estimation with limited dynamic range

The work in [KH19a] deals with the estimation of Large-Scale Parameter (LSP) of radio channels when there is insufficient dynamic range. Large path loss for example can cause *outage*, meaning that the received signal power is smaller than the measurement noise floor. Often outage samples are not considered for LSP estimation. A more truthful approach would be to include outage samples in the LSP estimation, but with the notion that the sample value is unknown and *censored* by the measurement noise floor. The mean and standard deviation of the LSPs (path loss, shadow fading, and delay and angular spread) are estimated with a modified log-likelihood function that accounts for interval censoring of received power due to limited dynamic range. The estimation method is applied to outdoor-to-indoor measurements in the 14-14.5 GHz range.